ACS OMEGA

http://pubs.acs.org/journal/acsodf

Article

Prediction of •OH-Initiated and •NO_3-Initiated Transformation Products of Polycyclic Aromatic Hydrocarbons by Electronic Structure Approaches

Xue−Mei Chen,* Hao-Ran Li, Xi−Lai Feng, Hao-Tong Wang, and Xu-Hui Sun

Cite This: *ACS Omega* 2022, 7, 24942−24950

Read Online

ACCESS | Metrics & More | Article Recommendations | Supporting Information

ABSTRACT: The abiotic reaction products of polycyclic aromatic hydrocarbons (PAHs) with hydroxyl radicals (•OH) and nitrate radicals (•NO_3) are nitro-, oxygen-, and hydroxyl-containing PAHs (NPAHs, OPAHs, and OHPAHs). Four methods of the highest occupied molecular orbital (HOMO), Fukui function (FF), dual descriptor (DD), and population of π electrons (PP-π) are selected to predict the chemical reactivity of PAHs attacked by •OH and •NO_3 in this study. The predicted •OH-initiated and •NO_3-initiated transformation products are compared with the main PAH transformation products (PAH-TPs) observed in the laboratory. The results indicate that PP-π and DD approaches fail to predict the transformation products of fused PAHs containing five-membered rings. By predicting the PAH-TPs of 13−14 out of the 15 parent PAHs accurately, HOMO and FF methods were shown to be suitable for predicting the transformation products formed from the abiotic reactions of fused PAHs with •OH and •NO_3.

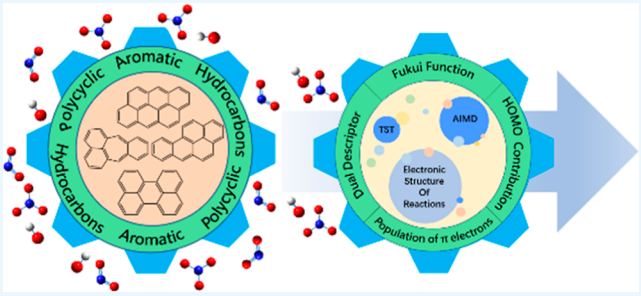

1. INTRODUCTION

Polycyclic aromatic hydrocarbons (PAHs) with high potential mutagenicity and carcinogenicity are the main byproducts in several incomplete combustion processes.[1−3] The persistent PAHs are spread into the atmosphere and deposited into soil and water,[4−9] which causes irreparable damage to human health and ecosystems.[7,10,11] Most scientific literature studies focus on the 16 priority PAHs defined by the United States Environmental Protection Agency (USEPA).[12] A significant amount of work[13−17] has reported on the abiotic reactions of PAHs with atmospheric oxidants of hydroxyl radicals (•OH) and nitro radicals (•NO_3) in the presence of O_2 and NO_x. The dominant mechanism involves electrophilic addition of •OH and •NO_3 to the aromatic ring, which results in the formation of nitro-PAHs (NPAHs), hydroxyl-PAHs (OHPAHs), and oxy-PAHs (OPAHs).[18,19] However, the presence of numerous isomers and the absence of some standards prevented the laboratory to identify some new PAH transformation products (PAH-TPs).[20] It is very necessary to find a robust method to predict the addition sites and potential PAH-TPs.

Three kinds of approaches, including ab initio theory,[21] transition-state (TS) theory,[22] and electronic structure of reactants[23] can be used to predict the reactive sites. The ab initio dynamics simulation fully considering various effects in the calculation is accurate and reliable but costs high computational resource and time. The TS theory can predict a specific reactive site and has previously been applied to predict potential PAH-TPs for a few PAHs.[24−31] It accurately predicted the potential PAH-TPs and explains the mechanism, but it is rather cumbersome to search the TS. A class of methods based on the electronic structure of reactants, including orbital composition,[32,33] Fukui function (FF),[34,35] dual descriptor (DD),[36−38] atomic charge,[39,40] electrostatic potential,[41] average local ionization energy (ALIE), and so forth,[42] have been extensively applied to different reaction systems and are very convenient for calculation and analysis. The regioselectivity, electrophilicity, and nucleophilicity of various reactants have been successfully predicted by DD and FF methods.[43−51] ALIE has been adapted for the study of quantitative structure−property.[52−54] Ivan A. Titaley et al.[52] pointed out that ALIE performed well in predicting the reactivity of 12 out of 15 PAHs. Lu tian et al.[32] suggested that FF, ALIE, and DD methods were suited for mono- and disubstituted benzenes with ortho- and para-directing groups. Highest occupied molecular orbital (HOMO) compositions have been applied to surface analysis and quantum mechanical studies.[54−60] In this framework, the convenient methods based on the electronic structure of PAHs can be used as

Received: November 15, 2021
Accepted: July 1, 2022
Published: July 13, 2022

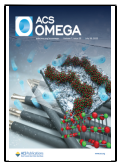

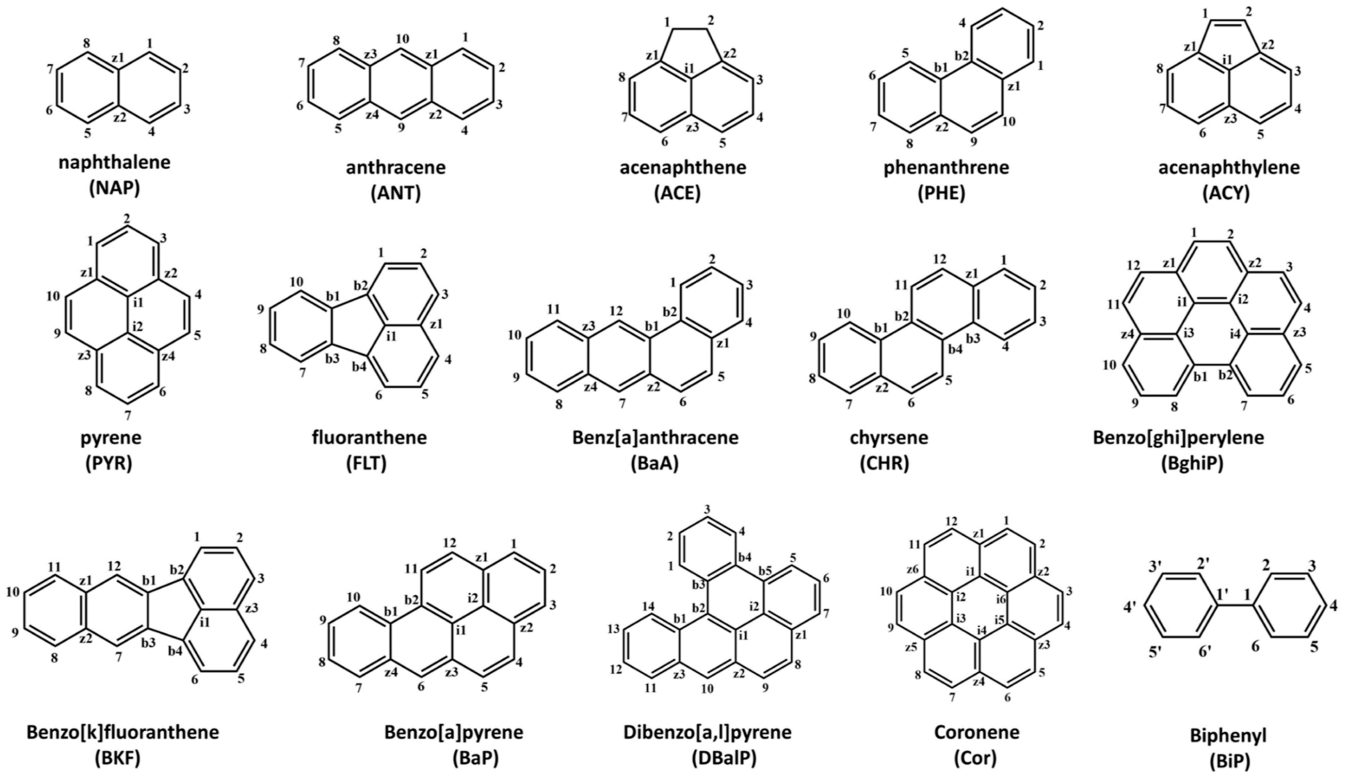

Figure 1. Structures and relevant numberings of the 15 parent PAHs.

Table 1. Substitution Sites of the 15 Parent PAHs Based on the Predictive Approaches and Laboratory Data[a]

PAHs	PP-π	FF	DD	HOMO	laboratory NPAHs	laboratory OPAHs and OHPAHs
NAP	C1, C2	C1, C2	C1, C2	C1, C2	C1^{m},g, C2	C1^{m},g, C2
ANT	C9, C1	C9, C1	C9, C1	C9, C1	C9^{m},g,p, C1	C9^{m},g,p
ACE	C3, C5	C5, C3	C5, C3	C5, C3	C4^{m},g, C3, C5,	C5^{m},g,p, C4, C3, C1
PHE	C9, C1	C9, C1	C9, C1	C9, C3	C9^{m},g, C3	C9^{m},g,p,C1,C3
ACY	Ci1, C1	C1, Ci1	Ci1, C4	C1, Ci1	C4^{m},g,C1	C1^{m},g,p
PYR	C1, C4	C1, C4	C1, C4	C1, C4	C1^{m},p, C4m,g, C2	C1^{m},g,p
FLT	Cb1, C3	C3, Cb4	Cb4, C8	C3, Cb4	C2^{m},p, C3m,g, C8, C7	
BaA	C7, C12	C7, C12	C7, C6	C7, C12	C7^{m},p	C7^{m},p, C12
CHR	C5, C4	C6, Cb2	C6, C1	C6/C12, Cb2	C6^{m},p	
Cor	C1/C7	C1/C7	C1/C7	C1/C7		C1^{m},p
Bghip	C7/C1, C5	C7, C5	C5/C4, C1	C5, C4	C5^{m},p, C7, C4	
BKF	C7/C8, C2	C7, C3	C6, Ci1	C7, C3	C7^{m},p, C3, C8, C1, C9	
BaP	C6, C1/C3	C6, C1/C3	C6, C1/C3	C6, C1/C3	C6^{m},p, C1, C3	C6^{m},p, C1, C3
DBalP	C10, C7	C10, Cb2	C10/C7	C10, Cb2	C10^{m},p	
BIP	C2, C6	C4, C2	C4, C2	C4, C1	C3^{m},g	

[a]The carbons before "," in the four theoretical method columns are the most reactive sites. The reactivity of the two carbons before and after "/" is equal, "m" indicates the major product, and "g" and "p" are the abbreviations of the gas and particle phase. "-" indicates that no product has been previously detected in the laboratory.

complementary approaches to predict the formation of PAH-TPs in laboratory studies and to guide further analysis in combination with experiments.

In this study, 15 parent PAHs shown in Figure 1 are selected as the test sets. Four prediction approaches based on the electronic structure are used to predict the reactivity of PAHs attacked by $^{\bullet}OH$ and $^{\bullet}NO_3$, which are the HOMO,[32,33] FF, DD, and population of π electrons (PP-π).[61] Although these methods have been extensively applied to different reaction systems, the plausibility and reliability of predictions in the parent PAHs system attacked by $^{\bullet}OH$ and $^{\bullet}NO_3$ remain to be explored and compared. In particular, the DD and PP-π methods have never been applied to predict the reactivity of atmospheric parent PAHs. The purpose of the study is to evaluate the performance of the four methods in predicting the reactivity of PAHs attacked by $^{\bullet}OH$ and $^{\bullet}NO_3$ in the presence of O_2 and NO_x and seek a robust and general prediction approach to help discover new PAH-TPs that have not yet been studied in the laboratory, enhancing the understanding of the formations of atmospheric PAH-TPs.

2. RESULTS AND DISCUSSION

2.1. Prediction of PAH Reactivity-Based Population of π Electrons. The population analysis of π electrons was

https://doi.org/10.1021/acsomega.1c06447
ACS Omega 2022, 7, 24942−24950

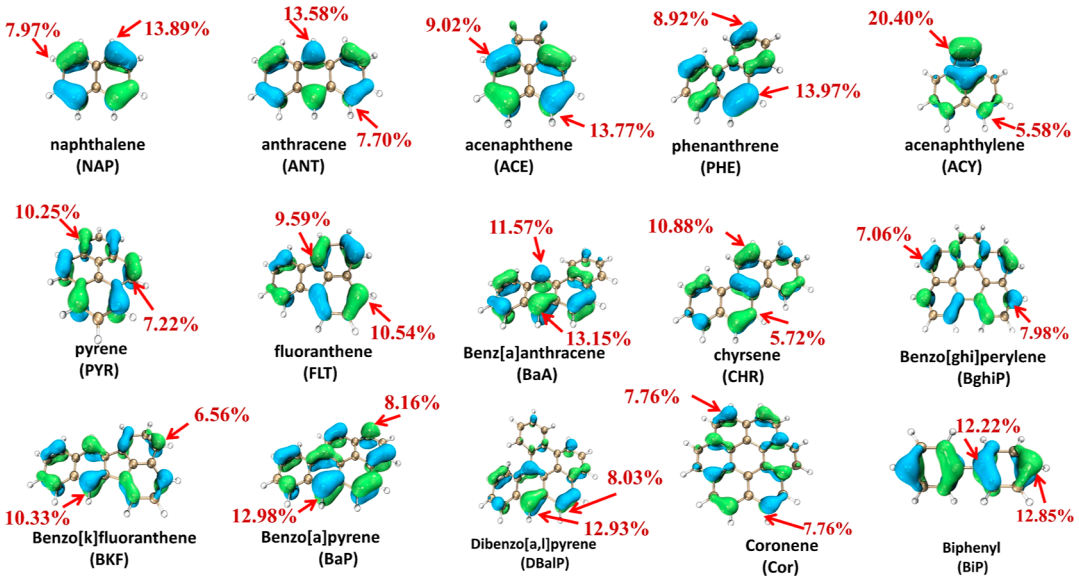

Figure 2. HOMO composition of the 15 parent PAHs. For clarity, only the top two contribution values are illustrated.

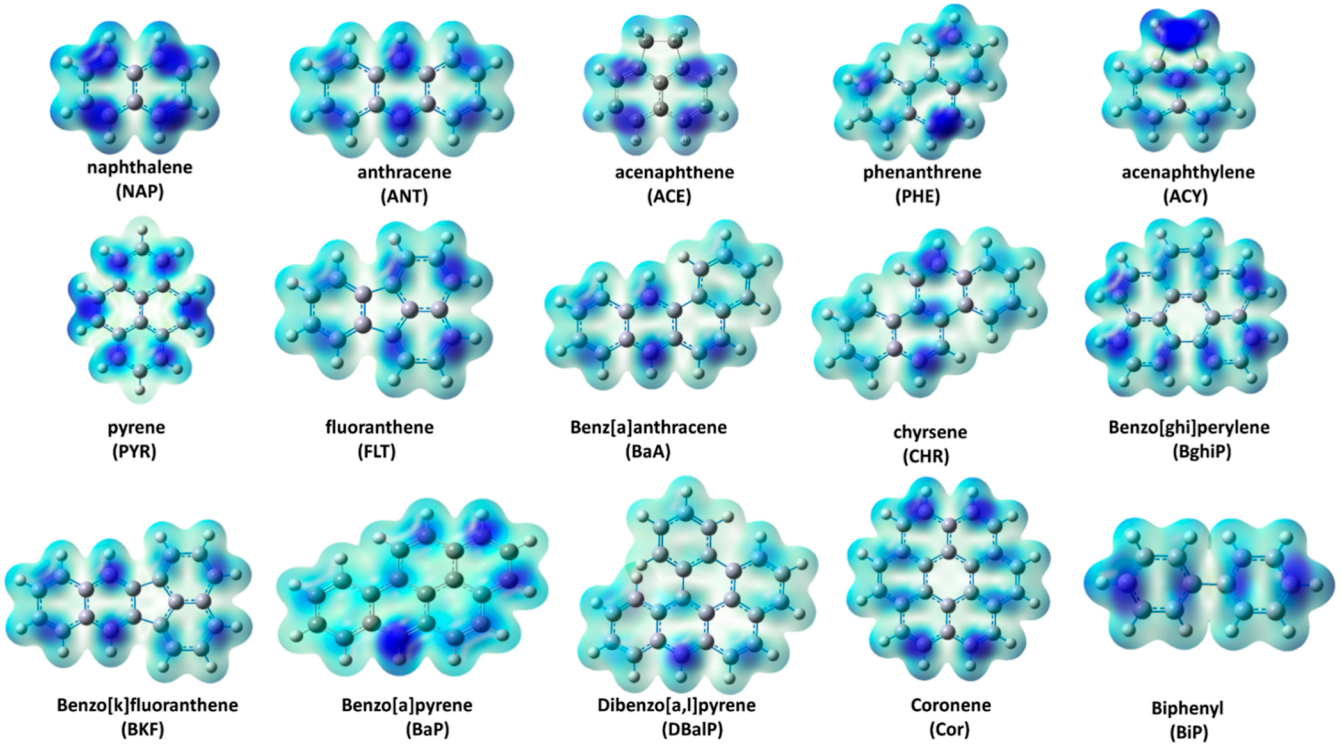

Figure 3. FF isosurfaces of the 15 parent PAHs. The darkest blue locations are favorable reactive sites for the radical attack.

performed to predict the reactivity of 15 PAHs attacked by $^{\bullet}OH$ and $^{\bullet}NO_3$, and the results are shown in Table S1. The combined results of the reactivity predictions and laboratory data (Table 1) indicate that the predicted reactive carbon atoms match with the transformation products in the laboratory[62−64] for nine parent PAHs, including NAP, ANT, PHE, PYR, BaA, Cor, BaP, Bghip, and DBalP. A previous study[63] reported that the gas-phase OHPAH and NPAH products of PHE were formed at the C9 atom, demonstrating the accuracy of the predicted result. The C7 atom of BaA is predicted to be the most reactive atom, which is consistent with experimental product 7-nitrobenzo[a]anthracene.[65] The only other reactive atom of BaA is predicted to be on the C12 atom, which matches with the reported di-OBaA and di-OHBaA products, 7,12-benzo[a]anthracenedione and 7,12-hydroxybenz[a]anthrone, respectively.[13,65] The major product 1,7-dihydroxycoronene observed in the laboratory also matches with the predicted reactivity of Cor.[66] The population analysis of π electrons cannot correctly predict the reactivity of CHR.[67]

The PP-π method performs poorly in predicting the reactive sites of fused PAHs with five-membered rings, such as ACE, ACY, FLT, and BKF. The most reactive site of ACY is predicted to be on the bridge carbon atom Ci1, which is not corresponding with the major NACY product 4-nitroacenaph-

https://doi.org/10.1021/acsomega.1c06447
ACS Omega 2022, 7, 24942−24950

thylene.[68] The predicted reactivity of Cb1 in FLT does not match with the transformation products 3-NFLT and 2-NFLT.[69,70] Therefore, the π electron population method that excludes the σ electrons is not suitable to predict the reactivity of fused PAHs containing five-membered rings. The PP-π method is also not a good choice for unfused biphenyl.

2.2. Prediction of PAH Reactivity-Based HOMO. The HOMO composition of the 15 parent PAHs is calculated. The contribution of each carbon atom to HOMO is listed in Table S2, and the top two contribution values are illustrated in Figure 2. With few exceptions, the predictions are consistent with the products identified in the laboratory.

The reactive carbon atoms of the fused PAHs with six-membered rings are predicted based on HOMO compositions. For ANT, the highest contribution to HOMO is at C9 (C10) with 13.58%, followed by C1 with 7.70%. The prediction is consistent with 9-nitroanthracene (9-NANT) and 9,10-anthraquinone, meanwhile, and the experimental transformation products occurred at C1 correspond to the reactivity order of ANT.[71] The reactive sites of BaA are predicted to be at C7 (13.15%) and C12 (11.57%), and the product benz[a]-anthracene-7,12-dione[62,65] obtained in the experiment confirms the accuracy of the prediction. The successive reaction sites predicted for BghiP are at C5 (7.98%), C4 (7.06%), and C7 (6.80%), which are consistent with the products observed in the laboratory, such as 5-, 7-, and 4-nitrobenzo[ghi]-perylene.[62] The respective identified products of DBalP, CHR, and Cor are 1,10-dihydroxycoronene, 6-nitrodibenzo[a,l]-pyrene, and 6-nitrochrysene,[62,66] which is corresponding to the predictions.

The ACY-containing unsaturated cyclopenta-fused ring presents a unique reactivity pattern.[52] The experimentally observed OHACY adduct[15] supports the prediction that OH addition to ACY occurs at C1(C2), which accords with the higher reactivity of the double bond between C1 and C2. However, the prediction of C1(C2) is not in accord with 4-nitroacenaphthylene (4-NACY) identified in the laboratory, which was produced from indirect nitrate radical addition to ACY.[15] Nitrate radical addition to the C1−C2 bond is considered to be the dominant reaction pathway for ACY with the substituent groups.[72]

For PAHs with different transformation products in the particle and gas phase, the HOMO method is effective to one of the two phases. For FLT, the highest contribution of C3 to HOMO matches with 3-nitrofluoranthene as the gas-phase product.[73] The most reactive site of PYR is predicted to be at C1 (10.25%), which is consistent with the major gas-phase NPYR and OHPYR; however, the other reactive atom C4 (7.22%) of PYR is in accord with the major particle-phase NPYR product16.[16,74]

2.3. Prediction of PAH Reactivity-Based FF. The FF isosurfaces of the 15 PAHs in the test sets and the CFF value of each carbon atom are shown in Figure 3 and Table S3, respectively. The CFF values and the darkest blue location on the isosurfaces suggest the reactivity of 15 parent PAHs attacked by $^{\bullet}OH$ and $^{\bullet}NO_3$, and the predictions are in good agreement with the published laboratory products.

The results predicted by the FF method are almost consistent with those predicted by the HOMO method. Except for BghiP, the FF method predicts the reactivity of all the fused PAHs with six-membered rings as successfully as the HOMO method. A few previous studies[62] reported that 5-NBghiP was the dominant nitro product formed from the reaction of BghiP with NO_2/NO_3; however, the FF method predicts C7 to be the most reactive atom. The FF method generally performs well in predicting the reactivity of fused PAHs with five-membered rings. C5 is predicted to be the most reactive site of ACE, which is consistent with the observed 5-nitroacenaphthene as the major product resulting from the $^{\bullet}OH$-initiated reaction of ACE.[75,76] 4-Nitroacenaphthene identified as the major product formed from the N_2O_5+ACE reaction was not expected to the significant ambient product since $^{\bullet}NO_3$ totally dominates over N_2O_5 under ambient atmospheric conditions. The major mono-NPAH products of BKF and FLT (7-nitrobenzo[k]-fluoranthene[62] and 2-nitrofluoranthene[73]) also support the prediction results that the C7 atom of BKF and the C3 atom of FLT are the most reactive, respectively.

The selectivity order of the predicted BKF using FF and HOMO methods is C7 > C3 > C8, which agrees with the reported yields of mono-nitro and di-nitro BKF products.[62] 7-Nitrobenzo[k]fluoranthene (7-NBKF) rather than 3-nitrobenzo[k]fluoranthene (3-NBKF) was identified as the major mono-NBKF product in a previous study; meanwhile, further nitration was proved to occur on C3, leading to the formation of 3,7-diNBKF.[62] Moreover, the predicted selectivity order of BaP is C6>C1/C3>C12, which is consistent with BaP-1,6-dione, BaP-3,6-dione, and BaP-6,12-dione being the major OPAH adducts of BaP.[77] The predicted reactivity orders of NAP, ANT, PHE, BaA, ACE, and PYR are also reasonable and reliable. Therefore, FF and HOMO methods are available to predict the selectivity order.

2.4. Prediction of PAH Reactivity Based on DD. The DD approach predicts the reaction selectivity of 15 parent PAHs attacked by $^{\bullet}OH$ and $^{\bullet}NO_3$, and the results indicate that the predicted reactivity for 10 fused PAHs with six-membered rings match well with the collected experimental results. For NAP, the NAP-OH adduct added by $^{\bullet}OH$ at the C1 or C2 site has been confirmed in multiple laboratorial and theoretical studies.[78,79] The energy-rich intermediate NAP-OH reacts with NO_2 in the atmosphere, and 1- and 2-nitronaphthalene, 2-hydroxy-1-nitronaphthalene, and 1-hydroxy-2-nitronaphthalene can be formed by the N atom attacking $^{\bullet}OH$ at the trans- or cis-position. 6-Nitrobenzo[a]pyrene obtained in laboratory studies[64] confirms that the C6 atom predicted by the DD method is the most reactive. The high CDD value of the C1 (C7) atom of Cor is consistent with the major Cor-TPs. The predicted PAH-TPs of PHE, BaA, and Bghip agree with the products[80] identified in the laboratory, respectively.

The DD method fails in predicting the reaction selectivity of ACY, FLT, and BKF. In the case of FLT, the most reactive site is predicted to be at the bridge carbon atom; however, the laboratory data indicated that particle-phase 3-NFLT and gas-phase 2-NFLT were the major FLT-TPs.[68,73,80] The major observed BKF-TPs (7-NBKF and 3,7-DiNBkF) in a previous experimental study[62] also suggested that the selectivity of BKF is not on the predicted C6 atom. Therefore, DD is an inappropriate method for fused PAHs with five-membered rings.

2.5. Evaluations of the Different Prediction Approaches. The numbers of correctly predicted primary substitution sites out of 15 parent PAHs attacked by $^{\bullet}OH$ and $^{\bullet}NO_3$ are shown in Figure 4. The PP-π approach is suitable to predict fused PAHs with six-membered rings but performs poorly for fused PAHs with five-membered rings and unfused polycyclic arene. Although the DD method accurately

https://doi.org/10.1021/acsomega.1c06447
ACS Omega 2022, 7, 24942−24950

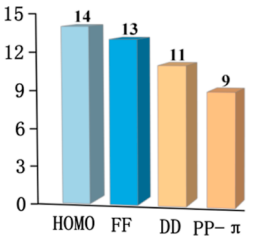

Figure 4. Number of correctly predicted primary substitution sites out of 15 parent PAHs attacked by $^{\bullet}OH$ and $^{\bullet}NO_3$.

predicted 11 PAH-TPs out of 15 parent PAHs, it is inappropriate for a vast majority of fused PAHs with five-membered rings. Based on the above prediction results, it is gratifying that the HOMO approach successfully predicts the transformation products of 14 parent PAHs, and the selectivity of PAHs can even be preliminarily estimated by the shape of HOMO. The FF method performs stably and accurately in predicting the reactivity of fused PAHs. The predicted selectivity order using HOMO and FF is also satisfied. The essence of $^{\bullet}OH$ and $^{\bullet}NO_3$ attacking parent PAHs is electrophilic addition, and the frontier orbital theory suggests that the electrophilic reactions relate to HOMO; thus, the HOMO and FF $[f^{-} \approx \rho_{HOMO}(r)]$ methods performed well, while the PP-π and DD methods failed to predict the reactive sites of PAHs containing five-membered rings. Therefore, HOMO and FF approaches are attractive and recommended to predict the abiotic transformation products of fused PAHs attacked by $^{\bullet}OH$ and $^{\bullet}NO_3$.

2.6. Predicting the Reactivity of Other PAHs Using HOMO and FF. In this study, 10 PAHs which have not yet been studied in the laboratory are selected as a prediction set, shown in Figure 5. In view of the outperformance in predicting the reactivity of parent PAHs, HOMO and FF approaches are used to predict the transformation products of the 10 PAHs attacked by $^{\bullet}OH$ and $^{\bullet}NO_3$. The predicted results are listed in Table 2.

Table 2. Predicted Results by HOMO and FF Methods for the 10 PAHs That Were Not Studied in the Laboratory

PAHs	HOMO	FF	PAHs	HOMO	FF
AHR	C3, C4/C6	C3, C4/C6	HEP	C3, C1	C3, C1
DBahA	C7, C5/C6	C7, C5/C6	AZU	C6, C2	C6, C7
PAC	C6, C5	C6, C5	PLE	C5, C6	C5, C6
PER	C1, C3	C1, C3	APT	C4, C6	C5, C4
PPH	C6, C5	C5, C6	BbF	C5, Cb2	C5, Ci1

The HOMO and FF methods predict that the reactivity order of AHR with six aromatic rings is C3 > C4 (C6); thus, 3-, 4-, and 6-nitroantanthrene and 3,4- and 3,6-antanthrene-quinone may be the major NAHR and OAHR products. In view of that AHR partition almost entirely into the particulate phase, the NAHR and OAHR products are in the particle phase. For DBahA, multiple reactive sites are predicted to be on C7 and C5 (C6) atoms, with C7 being the most reactive carbon. It can be inferred that the transformation products of DBahA are likely to be 5-, 6-, and 7-nitrodibenz[a,h]-anthracene, 5,6-, 6,7-, and 5,7-dibenz[a,h]anthracene-quinone, which agrees with the prediction by the ALIE approach.[35] The

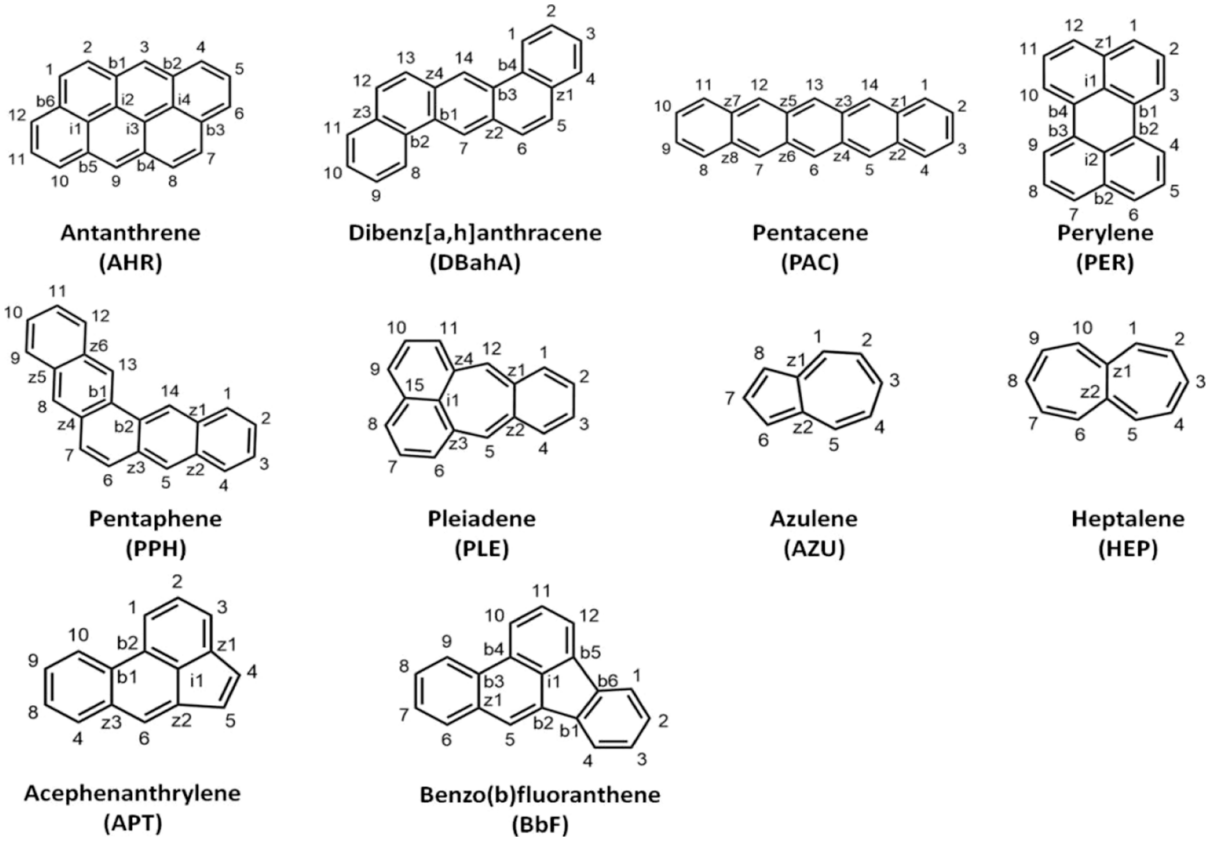

Figure 5. Structures and relevant numberings of 10 parent PAHs that have not been studied in the laboratory.

https://doi.org/10.1021/acsomega.1c06447
ACS Omega 2022, 7, 24942−24950

C6 and C5 atoms of PAC, the C1 and C3 atoms of PER, the C1 and C3 atoms of BeP, and the C5 and C6 atoms of PPH are the reactive sites, respectively. The predictions for the above fused PAHs with six-membered rings are supposed to be reliable. The reactive sites of the aromatic septet (HEP, AZU, and PLE) predicted by HOMO and FF agree with each other. To verify the accuracy of the predictions, the relative free energies of precursors, TSs, and adducts of •OH addition to AZU, PLE, and HEP were, respectively, calculated, and the results shown in Table S5 match well with the predictions by HOMO and FF. The most reactive site of HEP is predicted to be at the C3 atom; therefore, 3-nitroheptalene and 3-hydroxyheptalene are likely to be the major gas-phase products. 6-Nitroazulene and 5-nitropleiadene are the major predicted transformation products of AZU and PLE, respectively.

In summary, HOMO and FF approaches are effective to predict the selectivity and transformation products of fused PAHs attacked by •OH and NO_3 in the presence of O_2 and NO_x. The further discussions we suggest are (1) the validity of HOMO and FF in predicting the reactivity of methylated-, halogenated-, and heterocyclic PAHs and (2) the investigation of HOMO and FF on predicting the selectivity of PAHs with other atmospheric species such as the sulfate particle and chlorine.

3. COMPUTATIONAL METHODS

All geometry optimizations are performed with the Gaussian 09 software[81a] at the level of M06-2X[82]/6-311G(d,p) without any restriction on the symmetry. The M06-2X functional, a high-nonlocality functional with double the amount of nonlocal exchange, has demonstrated a good performance for the thermochemistry, kinetics, and weak interactions for the main group elements.[83,84] In view of that Minnesota functionals are especially prone to grid density issues, the M06-2X calculations reported here were done with the keywords "int = ultrafine" to improve the accuracy of the calculations. Given the high symmetry of many PAHs, the symmetrical carbon atoms are not discussed. All isosurface maps are rendered by the VMD 1.9.1 program[85] based on the cube files generated by MultiWFN.[86]

The population analysis of π electrons was performed for each of the PAHs. The population of πelectrons excludes the influence of σ electrons that have little influence on the electrophilic reaction of the conjugated system. More abundant π electrons indicate the larger population, the more likely to result in the electrophilic reaction. For PAHs with moreπelectrons, the PP-π approach may be helpful to improve the accuracy in predicting the electrophilic sites.[61]

The frontier orbital theory proposed by Kenichi Fukui suggests that the electrophilic reaction relates to HOMO, and the electrophilic site can be predicted by the HOMO composition of the substrate. The HOMO composition of parent PAHs is analyzed by the Hirshfeld[51,87,88] method. The atom with the highest contribution to HOMO is the most reactive site.

FF and DD are applied to predict the reactivity of parent PAHs. FF proposed by Parr and Yang[89] can be calculated unambiguously for three situations of nucleophilic attack f^+, electrophilic attack f^-, and neutral (radical) attack f^0.

$$f^- = \rho_N(r) - \rho_{N-1}(r) \approx \rho_{\mathrm{HOMO}}(r) \quad (1)$$

$$f^+ = \rho_{N+1}(r) - \rho_N(r) \approx \rho_{\mathrm{LUMO}}(r) \quad (2)$$

$$f^0 = \frac{f^+ + f^-}{2} \approx 1/2(\rho_{\mathrm{HOMO}}(r) + \rho_{\mathrm{LUMO}}(r)) \quad (3)$$

where ρ_N, ρ_{N+1}, and ρ_{N-1} represent the electron density of a system at the N electron state (containing N electrons), $N + 1$ electron state (gaining an electron), and $N - 1$ electron state (losing an electron), respectively. It is argued that the reactive site should have a larger value of FF than other regions; that is, regions with larger f^-, f^+, and f^0 are favorable for electrophilic, nucleophilic, and neutral (radical) attack, respectively. DD defined as $\Delta f = f^+ - f^-$ can simultaneously be used to investigate the electrophilic and nucleophilic reaction sites, so DD is more convenient than FF. If the distribution of Δf around site A is more positive than another site B, then one can say A is a more favorable site for nucleophilic attack than B, and in the meantime, B is a more preferential site for electrophilic attack than A.

The reactive regions on the molecular surface can be visualized via the isosurface graph of FF and DD; however, visual analysis is somewhat ambiguous and subjective. To quantify the discussions of FF and DD, namely, assigning a value for each atom to exhibit the extent that it can be acted as a reactive site, the "condensed" version of FF and DD based on population analysis techniques is calculated. The condensed Fukui function (CFF) can be calculated based on the atom charge for three situations of nucleophilic attack f_A^+, electrophilic attack f_A^-, and neutral (radical) attack f_A^0.

$$f_A^- = q_{N-1}^A - q_N^A \quad (4)$$

$$f_A^+ = q_N^A - q_{N+1}^A \quad (5)$$

$$f_A^0 = 1/2(q_{N-1}^A - q_{N+1}^A) \quad (6)$$

The condensed DD (CDD) based on atom charge can be calculated as follows

$$f_A^{(2)} = f_A^+ - f_A^- = 2q_N^A - q_{N+1}^A - q_{N-1}^A \quad (7)$$

The CFF and CDD based on Hirshfeld charge are used to predict the reactive sites in the study.

The compositionsof HOMO, CFF, and CDD and the population of π electrons are all calculated using the MultiWFN program.

■ ASSOCIATED CONTENT

Supporting Information

The Supporting Information is available free of charge at https://pubs.acs.org/doi/10.1021/acsomega.1c06447.

Population of π electrons of PAHs, compositions of HOMO of PAHs, CFF values, CDD values, calculated relative free energies, summarized main transformation products, major NPAHs, major OHPAHs and OPAHs, summarized laboratory studies, definition of orbital compositions and calculations, graphical outputs, optimized geometries, analysis results, and the optimized xyz coordinates for the relevant structures (PDF)

https://doi.org/10.1021/acsomega.1c06447
ACS Omega 2022, 7, 24942−24950

AUTHOR INFORMATION

Corresponding Author

Xue−Mei Chen − *College of Chemical Engineering, Northeast Electric Power University, Jilin City 132012, P. R. China;* orcid.org/0000-0003-3261-4835; Email: 534831110@qq.com

Authors

Hao-Ran Li − *College of Chemical Engineering, Northeast Electric Power University, Jilin City 132012, P. R. China*

Xi−Lai Feng − *College of Chemical Engineering, Northeast Electric Power University, Jilin City 132012, P. R. China*

Hao-Tong Wang − *College of Chemical Engineering, Northeast Electric Power University, Jilin City 132012, P. R. China*

Xu-Hui Sun − *College of Chemical Engineering, Northeast Electric Power University, Jilin City 132012, P. R. China*

Complete contact information is available at: https://pubs.acs.org/10.1021/acsomega.1c06447

Notes

The authors declare no competing financial interest.

ACKNOWLEDGMENTS

This work was funded by the Science and Technology Department of Jilin Province, China (2021023198SF).

REFERENCES

(1) Abdel-Shafy, H. I.; Mansour, M. S. A review on polycyclic aromatic hydrocarbons: source, environmental impact, effect on human health and remediation. *Egypt. J. Pet.* **2016**, *25*, 107−123.

(2) Haritash, A. K.; Kaushik, C. P. Biodegradation aspects of polycyclic aromatic hydrocarbons (pahs): a review. *J. Hazard. Mater.* **2009**, *169*, 1−15.

(3) Menzie, C. A.; Potocki, B. B.; Santodonato, J. Exposure to carcinogenic PAHs in the environment. *Environ. Sci. Technol.* **1992**, *26*, 1278−1284.

(4) Kong, S.; Yan, Q.; Zheng, H.; Liu, H.; Wang, W.; Zheng, S.; Yang, G.; Zheng, M.; Wu, J.; Qi, S.; Shen, G.; Tang, L.; Yin, Y.; Zhao, T.; Yu, H.; Liu, D.; Zhao, D.; Zhang, T.; Ruan, J.; Huang, M. Substantial reductions in ambient PAHs pollution and lives saved as a co-benefit of effective long-term PM2. 5 pollution controls. *Environ. Int.* **2018**, *114*, 266−279.

(5) Wang, W.; Jariyasopit, N.; Schrlau, J.; Jia, Y.; Tao, S.; Yu, T.-W.; Dashwood, R. H.; Zhang, W.; Wang, X.; Simonich, S. L. M. Concentration and photochemistry of PAHs, NPAHs, and OPAHs and toxicity of PM2. 5 during the Beijing Olympic Games. *Environ. Sci. Technol.* **2011**, *45*, 6887−6895.

(6) Liu, F.; Liu, J.; Chen, Q.; Wang, B.; Cao, Z. Pollution characteristics and ecological risk of polycyclic aromatic hydrocarbons (PAHs) in surface sediments of the southern part of the Haihe River system in China. *Chin. Sci. Bull.* **2013**, *58*, 3348−3356.

(7) Okona-Mensah, K.; Battershill, J.; Boobis, A.; Fielder, R. An approach to investigating the importance of high potency polycyclic aromatic hydrocarbons (PAHs) in the induction of lung cancer by air pollution. *Food Chem. Toxicol.* **2005**, *43*, 1103−1116.

(8) Wilcke, W. Synopsis polycyclic aromatic hydrocarbons (PAHs) in soil-a review. *J. Plant Nutr. Soil Sci.* **2000**, *163*, 229−248.

(9) Zhang, Y.; Zhang, L.; Huang, Z.; Li, Y.; Li, J.; Wu, N.; He, J.; Zhang, Z.; Liu, Y.; Niu, Z. Pollution of polycyclic aromatic hydrocarbons (PAHs) in drinking water of China: Composition, distribution and influencing factors. *Ecotoxicol. Environ. Saf.* **2019**, *177*, 108−116.

(10) Inomata, Y.; Kajino, M.; Sato, K.; Ohara, T.; Kurokawa, J.-I.; Ueda, H.; Tang, N.; Hayakawa, K.; Ohizumi, T.; Akimoto, H. Emission and atmospheric transport of particulate PAHs in Northeast Asia. *Environ. Sci. Technol.* **2012**, *46*, 4941−4949.

(11) Titaley, I. A.; Chlebowski, A.; Truong, L.; Tanguay, R. L.; Massey Simonich, S. L. Identification and toxicological evaluation of unsubstituted PAHs and novel PAH derivatives in pavement sealcoat products. *Environ. Sci. Technol. Lett.* **2016**, *3*, 234−242.

(12) Lundstedt, S.; White, P. A.; Lemieux, C. L.; Lynes, K. D.; Lambert, I. B.; Öberg, L.; Haglund, P.; Tysklind, M. Sources, fate, and toxic hazards of oxygenated polycyclic aromatic hydrocarbons (PAHs) at PAH-contaminated sites. *AMBIO A J. Hum. Environ.* **2007**, *36*, 475−485.

(13) Yao, J.-J.; Huang, Z.-H.; Masten, S. J. The ozonation of benz [a] anthracene: pathway and product identification. *Water Res.* **1998**, *32*, 3235−3244.

(14) Zeng, M.; Liao, Z.; Wang, L. Atmospheric oxidation of gaseous anthracene and phenanthrene initiated by OH radicals. *Atmos. Environ.* **2020**, *234*, 117587.

(15) Zhou, S.; Wenger, J. C. Kinetics and products of the gas-phase reactions of acenaphthylene with hydroxyl radicals, nitrate radicals and ozone. *Atmos. Environ.* **2013**, *75*, 103−112.

(16) Cochran, R. E.; Jeong, H.; Haddadi, S.; Fisseha Derseh, R. F.; Gowan, A.; Beránek, J.; Kubátová, A. Identification of products formed during the heterogeneous nitration and ozonation of polycyclic aromatic hydrocarbons. *Atmos. Environ.* **2016**, *128*, 92−103.

(17) Nikolaou, A.; Kostopoulou, M.; Lofrano, G.; Meric, S. Determination of PAHs in marine sediments: analytical methods and environmental concerns. *Global NEST J.* **2009**, *11*, 391−405.

(18) Tsapakis, M.; Stephanou, E. G. Diurnal cycle of PAHs, nitro-PAHs, and oxy-PAHs in a high oxidation capacity marine background atmosphere. *Environ. Sci. Technol.* **2007**, *41*, 8011−8017.

(19) Sabaté, J.; Bayona, J.; Solanas, A. Photolysis of PAHs in aqueous phase by UV irradiation. *Chemosphere* **2001**, *44*, 119−124.

(20) Kumar, B.; Verma, V.K.; Gaur, R.; Kumar, S.; Sharma, C. S.; Akolkar, A. B. Validation of HPLC method for determination of priority polycyclic aromatic hydrocarbons (PAHs) in waste water and sediments. *Adv. Appl. Sci. Res.* **2014**, *5*, 201−209.

(21) Tuckerman, M. E.; Ungar, P. J.; von Rosenvinge, T.; Klein, M. L. Ab initio molecular dynamics simulations. *J. Phys. Chem.* **1996**, *100*, 12878−12887.

(22) Esteves, P. M.; de M. Carneiro, M. J. W.; Cardoso, S. P.; Barbosa, A. G.; Laali, K. K.; Rasul, G.; Prakash, G. S.; Olah, G. A. Unified mechanistic concept of electrophilic aromatic nitration: convergence of computational results and experimental data. *J. Am. Chem. Soc.* **2003**, *125*, 4836−4849.

(23) Lu, T.; Chen, F. Calculation of molecular orbital composition. *Acta Chim. Sin.* **2011**, *69*, 2393−2406.

(24) Mao, X.; Wang, S.; Huang, Y.; Zhou, T. Theoretical Investigation of Gas Phase OH-Initiated Acenaphthylene Degradation Reaction. *Comput. Chem.* **2016**, *05*, 22−37.

(25) Qu, X.; Zhang, Q.; Wang, W. Theoretical Study on Mechanism for NO_3-Initiated Atmospheric Oxidation of Naphthalene. *Chem. Phys. Lett.* **2006**, *432*, 40−49.

(26) Qu, X.; Zhang, Q.; Wang, W. Mechanism for OH-Initiated Photooxidation of Naphthalene in the Presence of O_2 and NO_x: A DFT Study. *Chem. Phys. Lett.* **2006**, *429*, 77−85.

(27) Khanniche, S.; Louis, F.; Cantrel, L.; Černušák, I. Investigation of the Reaction Mechanism and Kinetics of Iodic Acid with OH Radical Using Quantum Chemistry. *ACS Earth Space Chem.* **2017**, *1*, 227−235.

(28) Khanniche, S.; Louis, F.; Cantrel, L.; Černušák, I. Thermochemistry of HIO_2 Species and Reactivity of Iodous Acid with OH Radical: A Computational Study. *ACS Earth Space Chem.* **2017**, *1*, 39−49.

(29) Magalhães, A. C. O.; Esteves da Silva, J. C. G.; Pinto da Silva, L. Density Functional Theory Calculation of the Absorption Properties of Brown Carbon Chromophores Generated by Catechol Heterogeneous Ozonolysis. *ACS Earth Space Chem.* **2017**, *1*, 353−360.

https://doi.org/10.1021/acsomega.1c06447
ACS Omega 2022, 7, 24942−24950

(30) Dang, J.; Shi, X.; Zhang, Q.; Hu, J.; Chen, J.; Wang, W. Mechanistic and Kinetic Studies on the OH-Initiated Atmospheric Oxidation of Fluoranthene. *Sci. Total Environ.* **2014**, *490*, 639−646.
(31) Dang, J.; Shi, X.; Hu, J.; Chen, J.; Zhang, Q.; Wang, W. Mechanistic and Kinetic Studies on OH-Initiated Atmospheric Oxidation Degradation of Benzo[α]Pyrene in the Presence of O_2 and NO_x. *Chemosphere* **2015**, *119*, 387−393.
(32) Rong, F.; Tian, L.; Feiwu, C. Comparing methods for predicting the reactive site of electrophilic substitut. *Acta Phys.-Chim. Sin.* **2014**, *30*, 628−639.
(33) Fukui, K. Theory of Orientation and Stereoselection. *InOrientation and Stereoselection*; Springer: Berlin, 1970; Vol. *15*, pp 1−85.
(34) Sánchez-Márquez, J. New advances in conceptual-DFT: an alternative way to calculate the Fukui function and dual descriptor. *J. Mol. Model.* **2019**, *25*, 123.
(35) Yang, W.; Mortier, W. J. The use of global and local molecular parameters for the analysis of the gas-phase basicity of amines. *J. Am. Chem. Soc.* **1986**, *108*, 5708−5711.
(36) Morell, C.; Grand, A.; Toro-Labbé, A. New dual descriptor for chemical reactivity. *J. Phys. Chem. A* **2005**, *109*, 205−212.
(37) De Proft, F.; Forquet, V.; Ourri, B.; Chermette, H.; Geerlings, P.; Morell, C. Investigation of electron density changes at the onset of a chemical reaction using the state-specific dual descriptor from conceptual density functional theory. *Phys. Chem. Chem. Phys.* **2015**, *17*, 9359−9368.
(38) Martínez-Araya, J. I. Why is the dual descriptor a more accurate local reactivity descriptor than Fukui functions? *J. Math. Chem.* **2015**, *53*, 451−465.
(39) Mulliken, R. S. Electronic population analysis on LCAO−MO molecular wave functions. I. *J. Chem. Phys.* **1955**, *23*, 1833−1840.
(40) Christoffersen, R.; Baker, K. Electron population analysis. Gross atomic charges in molecules. *Chem. Phys. Lett.* **1971**, *8*, 4−9.
(41) Murray, J. S.; Politzer, P. The electrostatic potential: an overview. *Wiley Interdiscip. Rev.: Comput. Mol. Sci.* **2011**, *1*, 153−163.
(42) Politzer, P.; Murray, J. S.; Bulat, F. A. Average local ionization energy: a review. *J. Mol. Model.* **2010**, *16*, 1731−1742.
(43) Chen, X. M.; Chu, Y. J.; Liu, C. G. Degradation Mechanism of Benzo[a]pyrene Initiated by the OH Radical and ^{1} O ^{2} : An Insight from Density Functional Theory Calculations. *ACS Omega* **2020**, *5*, 25552−25560.
(44) Zamora, P.; Bieger, K.; Cuchillo, A.; Tello, A.; Muena, J. Theoretical determination of a reaction intermediate: Fukui function analysis, dual reactivity descriptor and activation energy. *J. Mol. Struct.* **2021**, *1227*, 129369.
(45) Vidhya, V.; Austine, A.; Arivazhagan, M. Molecular structure, aromaticity, vibrational investigation and dual descriptor for chemical reactivity on 1-chloroisoquinoline using quantum chemical studies. *Results Mater.* **2020**, *6*, 100097.
(46) Cao, J.; Ren, Q.; Chen, F.; Lu, T. Comparative study on the methods for predicting the reactive site of nucleophilic reaction. *Sci. China: Chem.* **2015**, *58*, 1845−1852.
(47) Yañez, O.; Báez-Grez, R.; Inostroza, D.; Pino-Rios, R.; Rabanal-León, W. A.; Contreras-García, J.; Cardenas, C.; Tiznado, W. K. A Fukui Function-Guided Method for Molecular Structure Prediction. *J. Chem. Inf. Model.* **2021**, *61*, 3955−3963.
(48) Martinez, C.; Rivera, J. L.; Herrera, R.; Rico, J. L.; Flores, N.; Rutiaga, J. G.; López, P. Evaluation of the chemical reactivity in lignin precursors using the Fukui function. *J. Mol. Model.* **2008**, *14*, 77−81.
(49) Pilepić, V.; Uršić, S. Nucleophilic reactivity of the nitroso group. Fukui function DFT calculations for nitrosobenzene and 2-methyl-2-nitrosopropane. *J. Mol. Struct.: THEOCHEM* **2001**, *538*, 41−49.
(50) Mu, L.; Fan, W.; Yuan, X. A.; Huang, C.; Li, D.; Bi, S. Mechanistic insights into the C (sp^3)-H heteroarylation of amides and Fukui function analysis of regioselectivity. *Mol. Catal.* **2021**, *502*, 111394.
(51) Wang, B.; Rong, C.; Chattaraj, P. K.; Liu, S. A comparative study to predict regioselectivity, electrophilicity and nucleophilicity with Fukui function and Hirshfeld charge. *Theor. Chem. Acc.* **2019**, *138*, 124.
(52) Titaley, I. A.; Walden, D. M.; Dorn, S. E.; Ogba, O. M.; Massey Simonich, S.; Cheong, H. Y. Evaluating Computational and Structural Approaches to Predict Transformation Products of Polycyclic Aromatic Hydrocarbons. *Environ. Sci. Technol.* **2018**, *53*, 1595−1607.
(53) Murray, J.; Abu-Awwad, F.; Politzer, P. Characterization of aromatic hydrocarbons by means of average local ionization energies on their molecular surfaces. *J. Mol. Struct.: THEOCHEM* **2000**, *501*−*502*, 241−250.
(54) Martin, J. W.; Hou, D.; Menon, A.; Pascazio, L.; Akroyd, J.; You, X.; Kraft, M. Reactivity of polycyclic aromatic hydrocarbon soot precursors: implications of localized π-radicals on rim-based pentagonal rings. *J. Phys. Chem. C* **2019**, *123*, 26673−26682.
(55) Arunagiri, C.; Anitha, A.; Subashini, A.; Selvakumar, S. S. X-ray crystal structure, vibrational spectroscopy, DFT calculations, electronic properties and Hirshfeld analysis of (E)-4-Bromo-N'-(2, 4-dihydroxy-benzylidene) benzohydrazide. *J. Mol. Struct.* **2018**, *1163*, 368−378.
(56) Luo, M.; Huang, B.; Xu, Z. J.; Liu, S. N.; Zhu, Z. X.; Zhang, J. X.; Meng, X. G. Structural investigation, Hirshfeld surface analysis and quantum mechanical study of two dicyanopyridine derivatives. *J. Mol. Struct.* **2021**, *1228*, 129748.
(57) Milenković, D.; Avdović, E.; Dimić, D.; Sudha, S.; Ramarajan, D.; Milanović, Ž.; Trifunović, S.; Marković, Z. S. Vibrational and Hirshfeld surface analyses, quantum chemical calculations, and molecular docking studies of coumarin derivative 3-(1-m-toluidinoethylidene)-chromane-2, 4-dione and its corresponding palladium (II) complex. *J. Mol. Struct.* **2020**, *1209*, 127935.
(58) Wang, Y.; Guan, J.; Mei, B.; Fan, M.; Lu, R.; Du, R.; Chen, K.; Yao, J.; Jiang, Z.; Li, H. Distribution of Spin Density on Phenoxyl Radicals Affects the Selectivity of Aerobic Oxygenation of Phenols. *Inorg. Chem.* **2020**, *59*, 3562−3569.
(59) Hayatgheybi, S.; Khosravi, H.; Zahedian Tejeneki, H.; Rominger, F.; Bijanzadeh, H. R.; Balalaie, S. Synthesis of N-(Isoquinolin-1-yl) sulfonamides via Ag_2O-Catalyzed Tandem Reaction of ortho-Alkynylbenzaldoximes with Benchtop Stabilized Ketenimines. *Org. Lett.* **2021**, *23*, 3524−3529.
(60) Mirzaei, S.; Khosravi, H. Predicting the regioselectivity of nucleophilic addition to arynes using frontier molecular orbital contribution analysis. *Tetrahedron Lett.* **2017**, *58*, 3362−3365.
(61) Lu, T.; Chen, Q. A simple method of identifying π orbitals for non-planar systems and a protocol of studying π electronic structure. *Theor. Chem. Acc.* **2020**, *139*, 25.
(62) Jariyasopit, N.; McIntosh, M.; Zimmermann, K.; Arey, J.; Atkinson, R.; Cheong, P. H.-Y.; Carter, R. G.; Yu, T.-W.; Dashwood, R. H.; Massey Simonich, S. L. Novel nitro-PAH formation from heterogeneous reactions of PAHs with NO_2, NO_3/N_2O_5, and OH radicals: prediction, laboratory studies, and mutagenicity. *Environ. Sci. Technol.* **2014**, *48*, 412−419.
(63) Barbas, J. T.; Sigman, M. E.; Dabestani, R. Photochemical Oxidation of Phenanthrene Sorbed on Silica Gel. *Environ. Sci. Technol.* **1996**, *30*, 1776−1780.
(64) Ringuet, J.; Albinet, A.; Leoz-Garziandia, E.; Budzinski, H.; Villenave, E. Reactivity of polycyclic aromatic compounds (PAHs, NPAHs and OPAHs) adsorbed on natural aerosol particles exposed to atmospheric oxidants. *Atmos. Environ.* **2012**, *61*, 15−22.
(65) Jang, M.; McDow, S. R. Products of Benz[a]anthracene Photodegradation in the Presence of Known Organic Constituents of Atmospheric AerosolsBenz[a]anthracene photodegradation in the presence of known organic constituents of atmospheric aerosols. *Environ. Sci. Technol.* **1995**, *29*, 2654−2660.
(66) Guennoun, Z.; Aupetit, C.; Mascetti, J. Photochemistry of coronene with water at 10 K: first tentative identification by infrared spectroscopy of oxygen containing coronene products. *Phys. Chem. Chem. Phys.* **2011**, *13*, 7340−7345.
(67) Jariyasopit, N.; Zimmermann, K.; Schrlau, J.; Arey, J.; Atkinson, R.; Yu, T. W.; Dashwood, R. H.; Tao, T.; Simonich, S. Heterogeneous reactions of particulate matter-bound PAHs and NPAHs with NO_3/

https://doi.org/10.1021/acsomega.1c06447
ACS Omega 2022, 7, 24942−24950

N_2O_5, OH radicals, and O_3 under simulated long-range atmospheric transport conditions: reactivity and mutagenicity. *Environ. Sci. Technol.* **2014**, *48*, 10155−10164.
(68) Zimmermann, K.; Jariyasopit, N.; Simonich, S.; Shu, T.; Arey, J. Formation of nitro-PAHs from the heterogeneous reaction of ambient particle-bound PAHs with $N_2O_5/NO_3/NO_2$. *Environ. Sci. Technol.* **2013**, *47*, 8434−8442.
(69) Arey, J.; Zielinska, B.; Atkinson, R.; Winer, A. M.; Ramdahl, T.; Pitts, J. N., Jr. The formation of nitro-PAH from the gas-phase reactions of fluoranthene and pyrene with the OH radical in the presence of NO_x. *Atmos. Environ.* **1986**, *20*, 2339−2345.
(70) Atkinson, R.; Arey, J.; Zielinska, B.; Aschmann, S. M. Kinetics and nitro-products of the gas-phase OH and NO_3 radical-initiated reactions of naphthalene, Fluoranthene, and pyrene. *Int. J. Chem. Kinet.* **1990**, *22*, 999−1014.
(71) Atkinson, R.; Arey, J. Atmospheric chemistry of gas-phase polycyclic aromatic hydrocarbons: formation of atmospheric mutagens. *Environ. Health Perspect.* **1994**, *102*, 117−126.
(72) Keyte, I. J.; Harrison, R. M.; Lammel, G. Chemical reactivity and long-range transport potential of polycyclic aromatic hydrocarbons - a review. *Chem. Soc. Rev.* **2013**, *42*, 9333−9391.
(73) Garcia, K. O.; Teixeira, E. C.; Agudelo-Castañeda, D. M.; Braga, M.; Alabarse, P. G.; Wiegand, F.; Kautzmann, R. M.; Silva, L. F. Assessment of nitro-polycyclic aromatic hydrocarbons in PM (1) near an area of heavy-duty traffic. *Sci. Total Environ.* **2014**, *479−480*, 57−65.
(74) Carrara, M.; Wolf, J.-C.; Niessner, R. Nitro-PAH formation studied by interacting artificially PAH-coated soot aerosol with NO_2 in the temperature range of 295−523K. *Atmos. Environ.* **2010**, *44*, 3878−3885.
(75) Wang, L.; Wang, L. Atmospheric oxidation mechanism of acenaphthene initiated by OH radicals. *Atmos. Environ.* **2020**, *243*, 117870−117875.
(76) Wilcke, W.; Kiesewetter, M.; Musa Bandowe, B. A. Microbial formation and degradation of oxygen-containing polycyclic aromatic hydrocarbons (OPAHs) in soil during short-term incubation. *Environ. Pollut.* **2014**, *184*, 385−390.
(77) Avagyan, R.; Nyström, R.; Boman, C.; Westerholm, R. Determination of hydroxylated polycyclic aromatic hydrocarbons by HPLC-photoionization tandem mass spectrometry in wood smoke particles and soil samples. *Anal. Bioanal. Chem.* **2015**, *407*, 4523−4534.
(78) Musa Bandowe, B. A.; Sobocka, J.; Wilcke, W. Oxygen-containing polycyclic aromatic hydrocarbons (OPAHs) in urban soils of Bratislava, Slovakia: patterns, relation to PAHs and vertical distribution. *Environ. Pollut.* **2011**, *159*, 539−549.
(79) Ma, Y.; Cheng, Y.; Qiu, X.; Lin, Y.; Cao, J.; Hu, D. A quantitative assessment of source contributions to fine particulate matter (PM2.5)-bound polycyclic aromatic hydrocarbons (PAHs) and their nitrated and hydroxylated derivatives in Hong Kong. *Environ. Pollut.* **2016**, *219*, 742−749.
(80) Bandowe, B. A. M.; Meusel, H. Nitrated polycyclic aromatic hydrocarbons (nitro-PAHs) in the environment - A review. *Sci. Total Environ.* **2017**, *581−582*, 237−257.
(81) (a) Frisch, M.; Trucks, G.; Schlegel, G.; Scuseria, G.; Robb, M.; Cheeseman, J.; Scalmani, G.; Barone, V.; Mennucci, B.; Petersson, G. *Gaussian 09, revision A. 02*; Gaussian, Inc.: Wallingford, CT, 2009. (b) Lee, C.; Yang, W.; Parr, R. G. Development of the Colle-Salvetti correlation-energy formula into a functional of the electron density. *Phys. Rev. B: Condens. Matter Mater. Phys.* **1988**, *37*, 785−789.
(82) Zhao, Y.; Truhlar, D. G. The M06 suite of density functionals for main group thermochemistry, thermochemical kinetics, noncovalent interactions, excited states, and transition elements: two new functionals and systematic testing of four M06-class functionals and 12 other functionals. *Theor. Chem. Acc.* **2008**, *120*, 215−241.
(83) Zasada, F.; Piskorz, W.; Stelmachowski, P.; Legutko, P.; Kotarba, A. Density Functional Theory Modeling and Time-of-Flight Secondary Ion Mass Spectrometric and X-ray Photoelectron Spectroscopic Investigations into Mechanistic Key Events of Coronene Oxidation: Toward Molecular Understanding of Soot Combustion. *J. Phys. Chem. C* **2015**, *119*, 6568−6580.
(84) Pople, J. A.; Gordon, M. Molecular orbital theory of the electronic structure of organic compounds. I. Substituent effects and dipole moments. *J. Am. Chem. Soc.* **1967**, *89*, 4253−4261.
(85) Humphrey, W.; Dalke, A.; Schulten, K. VMD: visual molecular dynamics. *J. Mol. Graphics* **1996**, *14*, 33−38.
(86) Tian, L.; Chen, F. Multiwfn A multifunctional wavefunction analyzer. *J. Comput. Chem.* **2012**, *33*, 580−592.
(87) Hirshfeld, F. L. Bonded-atom fragments for describing molecular charge densities. *Theor. Chim. Acta* **1977**, *44*, 129−138.
(88) Shu-Bin, L. Conceptual density functional theory and some recent developments. *Acta Phys.-Chim. Sin.* **2009**, *25*, 590−600.
(89) Parr, R. G.; Yang, W. Density functional approach to the frontier-electron theory of chemical reactivity. *J. Am. Chem. Soc.* **1984**, *106*, 4049−4050.

https://doi.org/10.1021/acsomega.1c06447
ACS Omega 2022, 7, 24942−24950